Electronic Supplementary Information

Targeted design leads to tunable photoluminescence from perylene dicarboxdiimide-poly(oxyalkylene)/siloxane hybrids for luminescent solar concentrators

Ilaria Meazzini,[a] Niamh Willis-Fox,[a] Camille Blayo,[a] Jochen Arlt,[b] Sébastien Clément[c] and Rachel C. Evans[a]

[a] *School of Chemistry and CRANN, Trinity College, The University of Dublin, Dublin 2, Ireland. E-mail: raevans@tcd.ie*

[b] *Collaborative Optical Spectroscopy, Micromanipulation and Imaging Centre (COSMIC) and SUPA, School of Physics and Astronomy, King's Buildings, University of Edinburgh, EH9 3JZ, U.K.*

[c] *Institut Charles Gerhardt – UMR 5253, Université de Montpellier – CC1701, Place Eugène Bataillon, F-34095 Montpellier Cedex 05, France.*

Table of Contents

1. Materials

Jeffamine T-403, Jeffamine T-5000 and Jeffamine D-4000 were a kind gift from Huntsman International (www.huntsman.com). *O,O'*-Bis(2-aminopropyl) polypropylene glycol-*block*-polyethylene glycol-*block*-polypropylene glycol (Jeffamine ED-600), 3-isocyanatopropyltriethoxysilane (ICPTES), ethanol (EtOH, HPLC grade), hydrochloric acid (37% puriss), potassium bromide (FTIR grade), tetrahydrofuran (THF, HPLC grade) and ethanol (anhydrous) were procured from Sigma Aldrich and used as received. 3-Aminopropyltriethoxysilane (98%) was purchased from Alfa Aesar and used as received.

2. Synthesis and characterisation of PDI-Sil

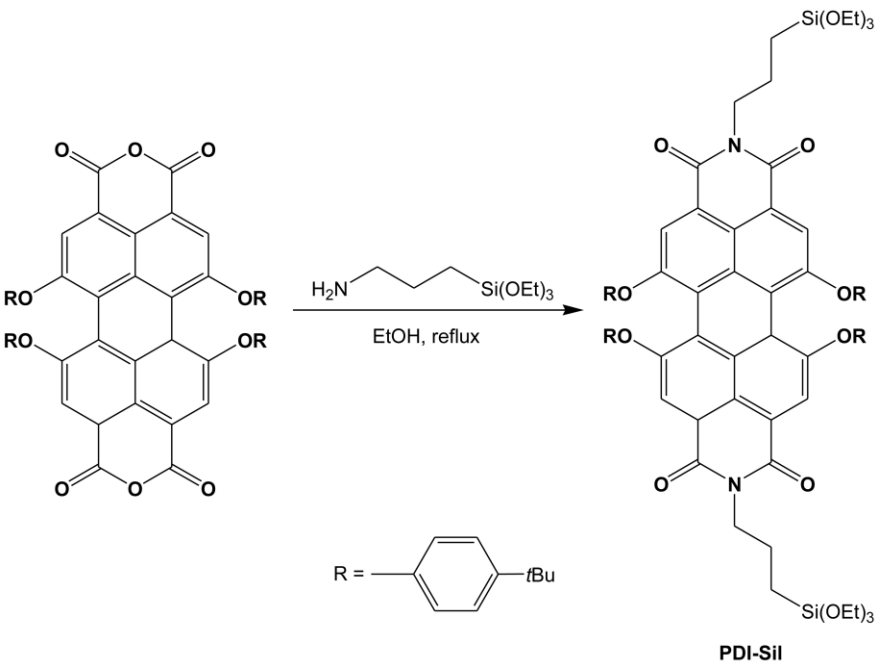

Figure S1. Synthetic route to **PDI-Sil**.

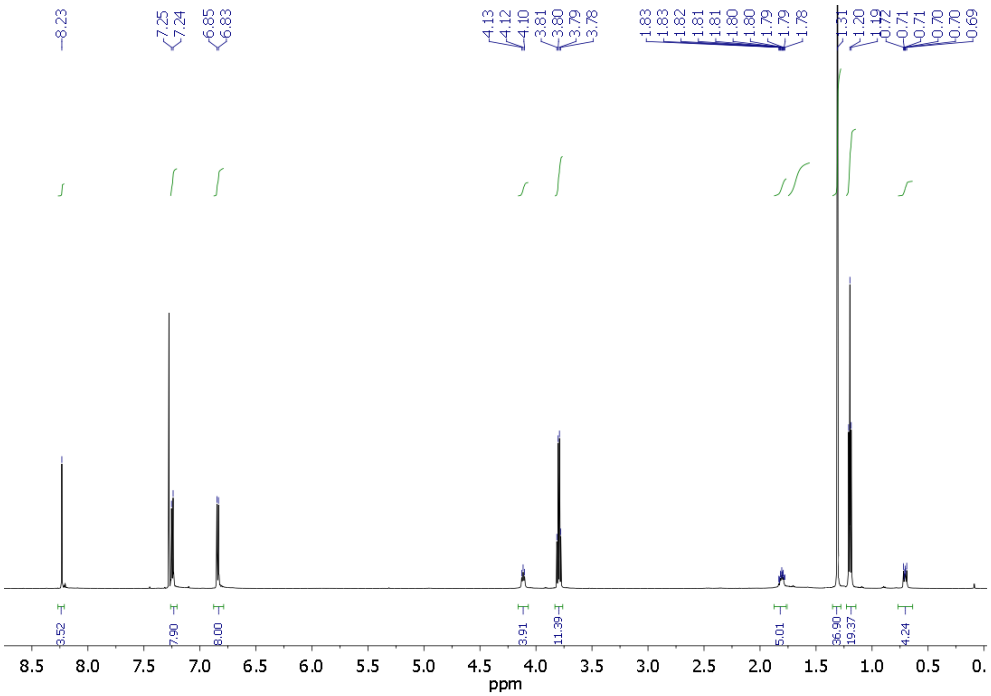

Figure S2. ^{1}H NMR spectrum of **PDI-Sil** in $CDCl_3$.

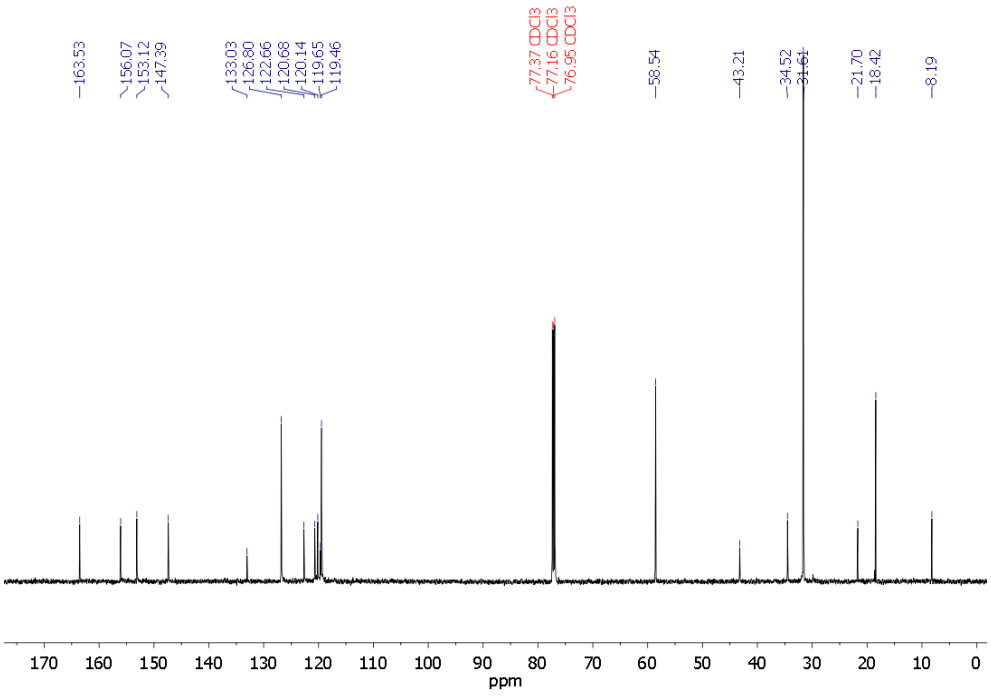

Figure S3. ^{13}C{^{1}H} NMR spectrum of **PDI-Sil** in $CDCl_3$.

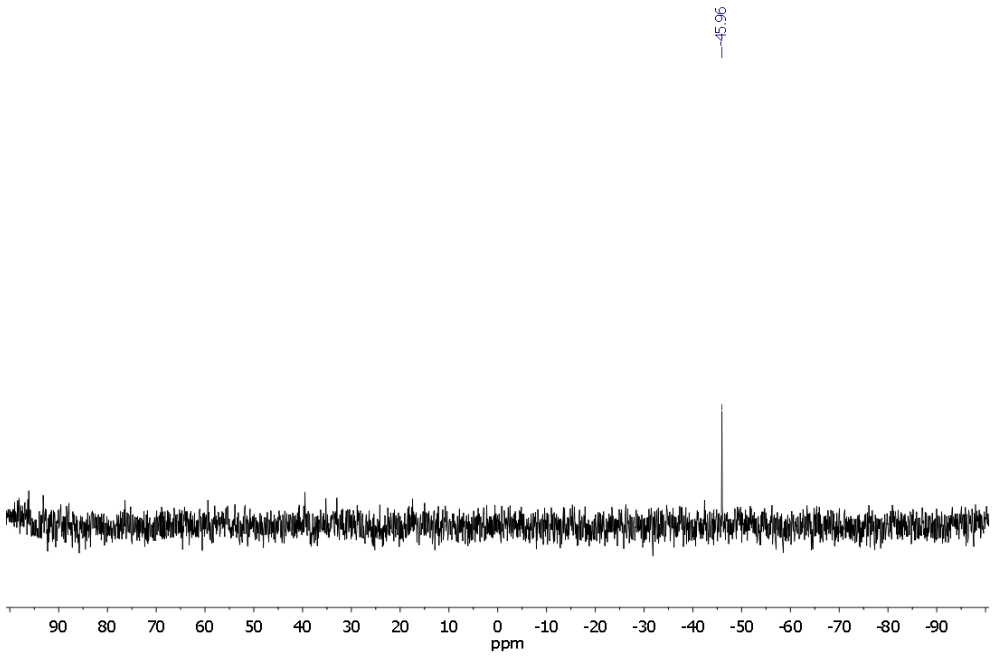

Figure S4. $^{29}Si\{^{1}H\}$ NMR spectrum of **PDI-Sil** in $CDCl_3$.

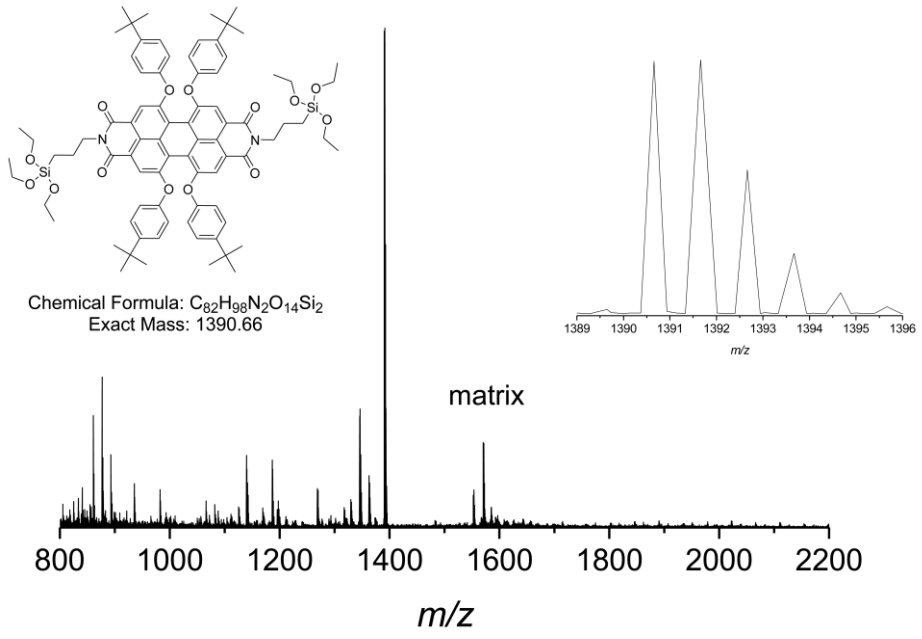

Figure S5. MALDI-MS of **PDI-Sil** in THF (0.7 mmol dm^{-3}).

3. Acidolysis Studies on PDI-Sil

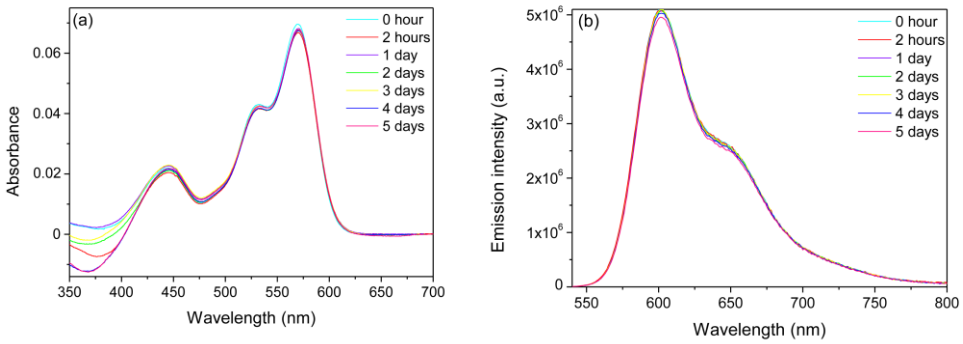

Figure S6. Absorption (a) and emission (b) spectra of **PDI-Sil** in THF (1×10^{-6} mol dm^{-3}) aged at pH 2 (λ_{ex} = 520 nm).

4. Local Structure Characterisation

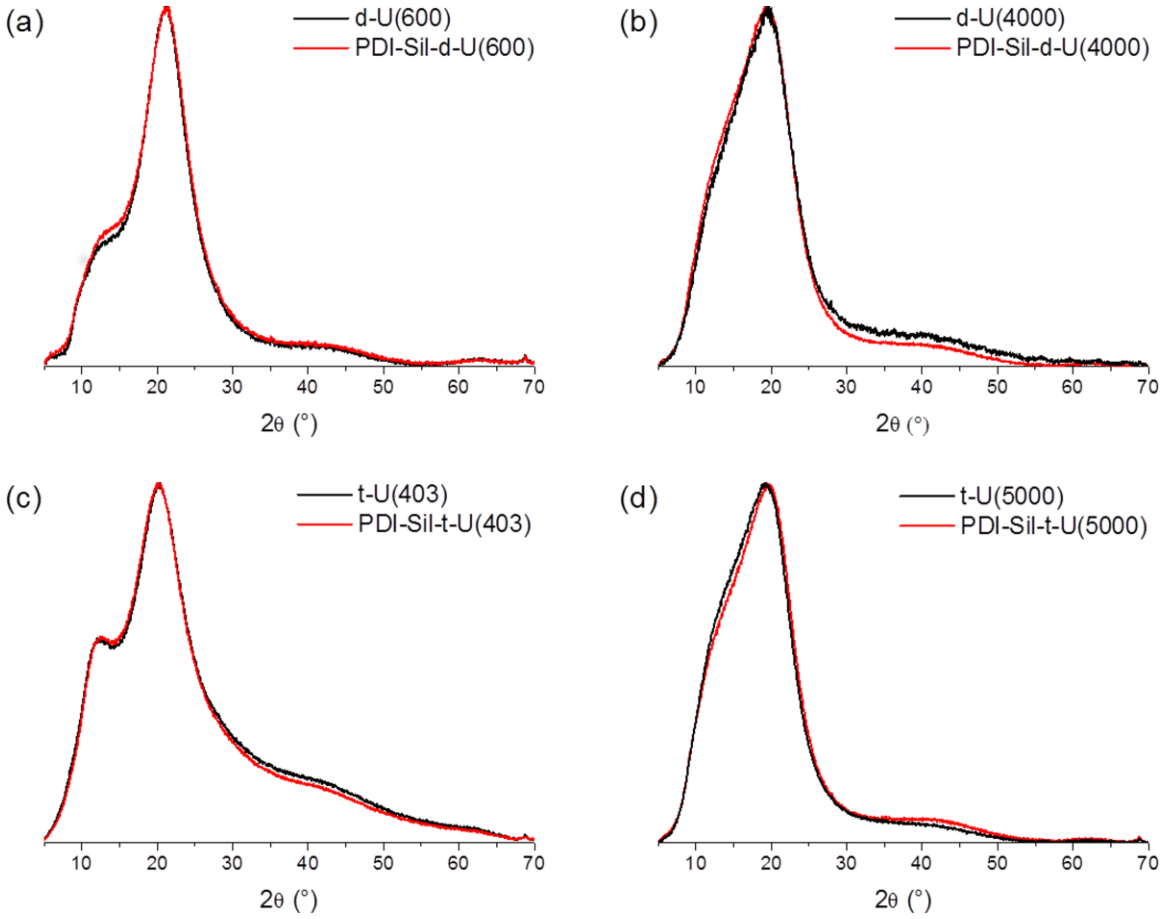

Figure S7. Powder X-ray diffraction patterns for (a) **d-U(600)** and **PDI-Sil-d-U(600)**, (b) **d-U(4000)** and **PDI-Sil-d-U(4000)**, (c) **t-U(403)** and **PDI-Sil-t-U(403)** and (d) **t-U(5000)** and **PDI-Sil-t-U(5000)**, in the range of 2θ = 5 – 70°.

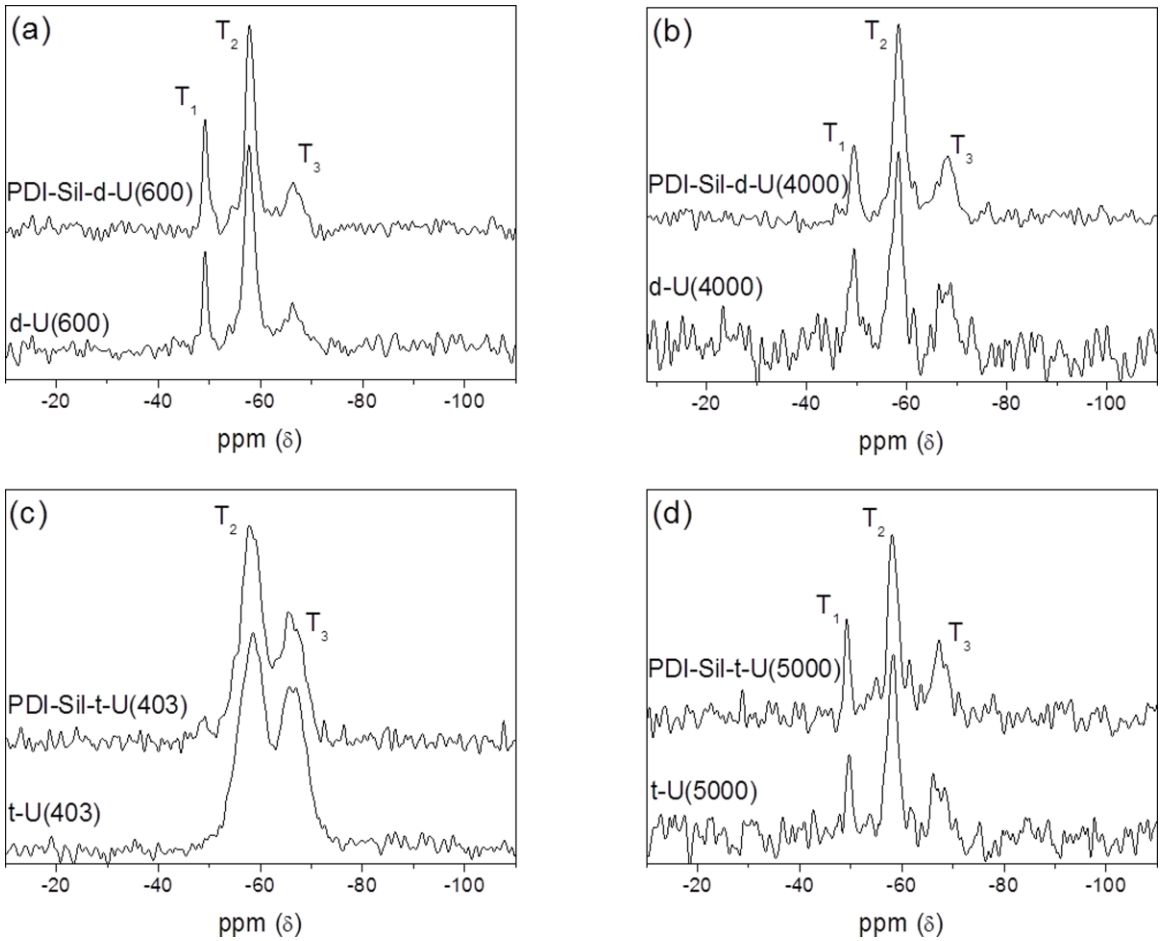

Figure S8. ^{29}Si solid-state MAS NMR spectra for (a) **d-U(600)** and **PDI-Sil-d-U(600**), (b) **d-U(4000)** and **PDI-Sil-d-U(4000)**, (c) **t-U(403)** and **PDI-Sil-t-U(403)** and (d) **t-U(5000)** and **PDI-Sil-t-U(5000)**.

Table S1. ^{29}Si MAS NMR chemical shifts (ppm vs TMS), population of different T_n species (%), T_n species ratios, and degree of condensation, *c* (%) of undoped and PDI-Sil-ureasils. Signals are labeled according to the T_n notation, where n (n = 1, 2, 3) is the number of Si-bridging oxygen atoms, T_1=(R′Si(OSi)-$(OR)_2$), T_2=(R′Si$(OSi)_2$(OR)), and T_3=(R′Si$(OSi)_3$).

Sample ID	T_1 (%)	T_2 (%)	T_3 (%)	T_1 : T_2 : T_3	*c (%)*[a]
d-U(600)	-49.2 (13.7)	-57.8 (59.8)	-65.8 (26.5)	1 : 4.4 : 1.9	71%
PDI-Sil-d-U(600)	49.2 (17.7)	-58.0 (58.3)	-66.1 (24.0)	1 : 3.3 : 1.4	69%
d-U(4000)	-49.3 (22.0)	-58.0 (54.0)	-67.9 (24.0)	1 : 2.5 : 1.1	67%
PDI-Sil-d-U(4000)	-49.5 (14.3)	-58.5 (57.3)	-67.8 (28.4)	1 : 4.0 : 2.0	71%
t-U(403)	_	-58.3 (57.5)	-66.5 (42.5)	0 : 1 : 0.7	81%
PDI-Sil-t-U(403)	_	-58.2 (61.4)	-67.2 (38.6)	0 : 1 : 0.6	80%
t-U(5000)	-49.7 (15.2)	-58.2 (60.1)	-67.2 (24.7)	1 : 4.0 : 1.6	70%
PDI-Sil-t-U(5000)	-49.3 (14.4)	-58.3 (53.9)	-67.3 (31.7)	1 : 3.7 : 2.2	72%

[a] $C = 1/3(\%T_1+2\%T_2+3\%T_3)$[1]

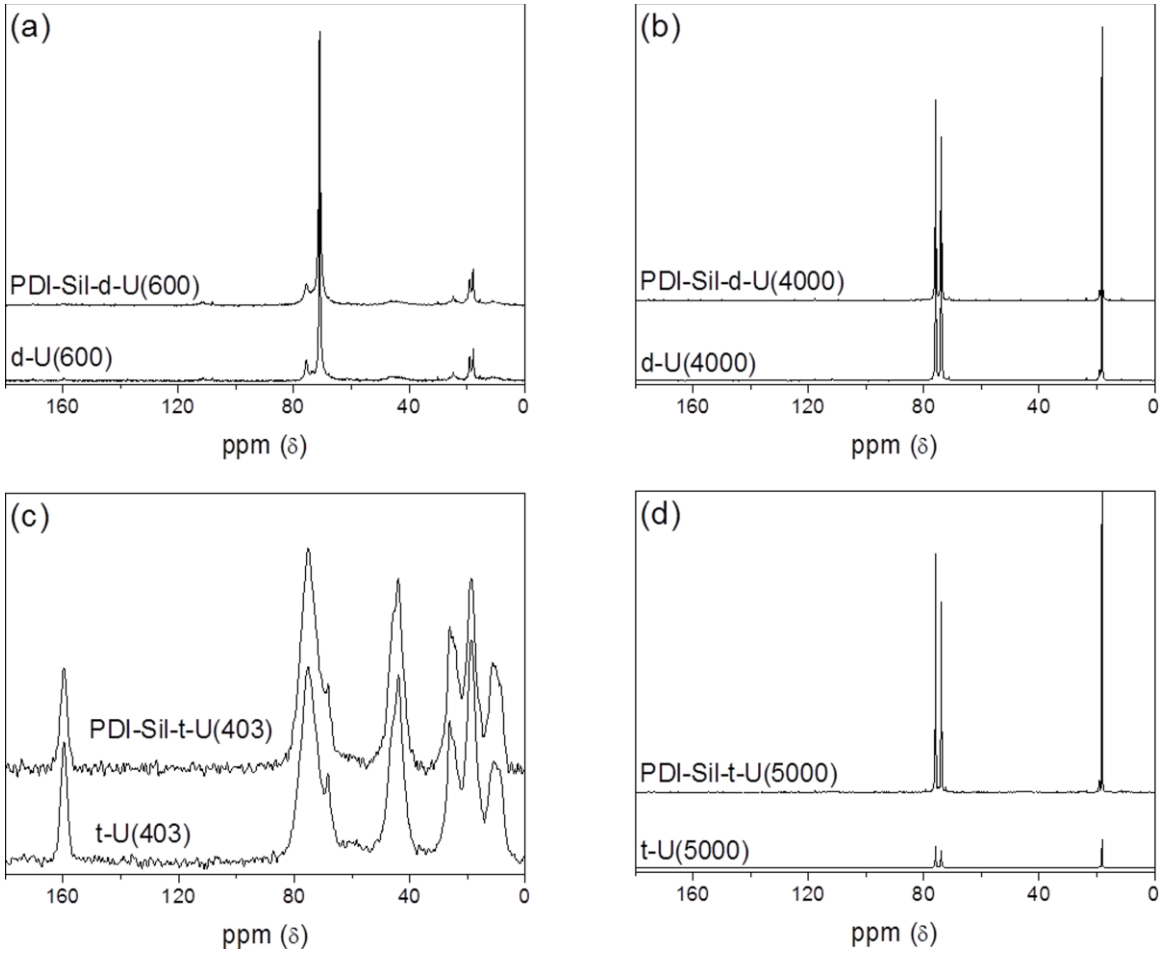

Figure S9. ^{13}C solid-state CP-MAS NMR spectra for (a) **d-U(600)** and **PDI-Sil-d-U(600),** (b) **d-U(4000)** and **PDI-Sil-d-U(4000),** (c) **t-U(403)** and **PDI-Sil-t-U(403)** and (d) **t-U(5000)** and **PDI-Sil-t-U(5000)**.

Table S2. ^{13}C solid-state CP-MAS NMR chemical shifts (ppm *vs.* TMS) of undoped and **PDI-Sil**-ureasils.

Signal Assignment	**d-U(600)**	**PDI-d-U(600)**	**d-U(4000)**	**PDI-Sil-d-U(4000)**	**t-U(403)**	**Sil-t-U(403)**	**t-U(5000)**	**PDI-Sil-t-U(5000)**
C=O urea	-	-	-	-	159.7	159.7	-	-
-OCH	75.7	75.7	74.0 / 75.9	74.0 / 75.9	75.3	75.2	74.1 / 75.9	74.0 / 75.9
-(OCH_2CH_2)-	71.0	71.0			68.3	68.3		
-NCH_2- in $N(CH_2)_3$-Si	45.8	45.3	-	-	43.9	44.0	-	-
-CH_2- in $N(CH_2)_3$-Si-	24.6	24.7	-	-	26.1	26.2	-	-
-CH_3 in $OCH_2CH(CH_3)$	19.1	19.0	19.0	19.1	18.8	18.7	19.0	19.1
-CH_3 in $(CH_3CH_2O)_3Si$	17.7	17.8	18.2	18.3	-	-	18.2	18.3
-CH_2Si- in $N(CH_2)_3Si$	-	-	-	-	10.9	11.4	-	-

Table S3. Results of Gaussian curve fitting of the 'amide I' band of undoped ureasils and PDI-Sil-ureasils, showing peak position, area and % contribution for each component resolved.

Sample ID	Peak 3 /cm^{-1} Contribution (%)	Peak 2 /cm^{-1} Contribution (%)	Peak 1 /cm^{-1} Contribution (%)	Peak 4 /cm^{-1} Contribution (%)	Peak 5 /cm^{-1} Contribution (%)
d-U(600)	1634.4 (20.75)	1662.5 (61.89)	1709.4 (12.32)	1758.1 (5.04)	-
PDI-Sil-d-U(600)	1635.2 (17.8)	1663.2 (59.61)	1708.5 (17.66)	1759.8 (4.93)	-
d-U(4000)	1635.3 (13.92)	1654.7 (77.25)	1707.1 (0.82)	1745.8 (5.13)	1727.3 (2.88)
PDI-Sil-d-U(4000)	1637.0 (22.10)	1657.4 (70.06)	1705.4 (1.00)	1743.7 (5.54)	1722.1 (1.30)
t-U(403)	1631.2 (25.16)	1658.3 (66.24)	1707.1 (6.37)	1742.9 (2.23)	-
PDI-Sil-t-U(403)	1633.2 (22.32)	1660.9 (65.83)	1707.0 (10.22)	1771.8 (1.63)	-
t-U(5000)	1636.5 (30.44)	1662.6 (56.32)	1716.0 (13.24)	-	-
PDI-Sil-t-U(5000)	1636.9 (23.44)	1658.1 (61.95)	1706.8 (13.56)	1747.0 (1.05)	-

5. Stability Studies

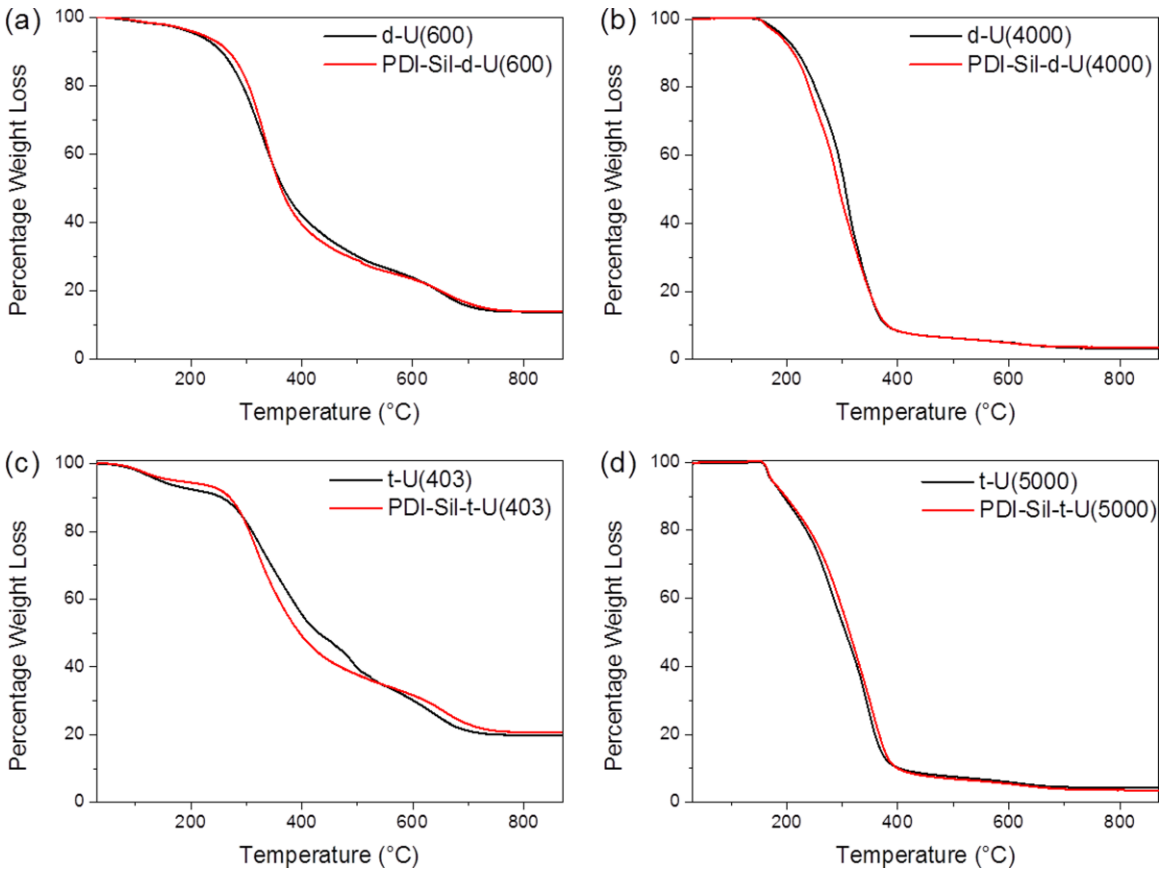

Figure S10. TGA thermograms of (a) **d-U(600)** and **PDI-Sil-d-U(600)**, (b) **d-U(4000)** and **PDI-Sil-d-U(4000)**, (c) **t-U(403)** and **PDI-Sil-t-U(403)** and (d) **t-U(5000)** and **PDI-Sil-t-U(5000)** (air atmosphere, 10° C min^{-1}).

Thermogravimetric analyses showed that the thermal decomposition of **d-U(600)** and **PDI-Sil-d-U(600)** occurs in a single step with an onset temperature of ~ 270 °C. While, a similar trend is observed for **d-U(4000)** and **PDI-Sil-d-U(4000)** (onset T~250 °C), **t-U(403)**-based hybrids, present a first weight loss between 30 to 190 °C, ascribed to the evaporation of un-reacted ICPTES and solvents and a second weight loss at an onset T of ~280 °C. The thermal degradations of **t-U(5000)** and **PDI-Sil-tU(5000)** occur in a singles step (onset T~280 °C). Overall, no change to the thermal profile of each ureasil is detected upon the grafting of the **PDI-Sil**.

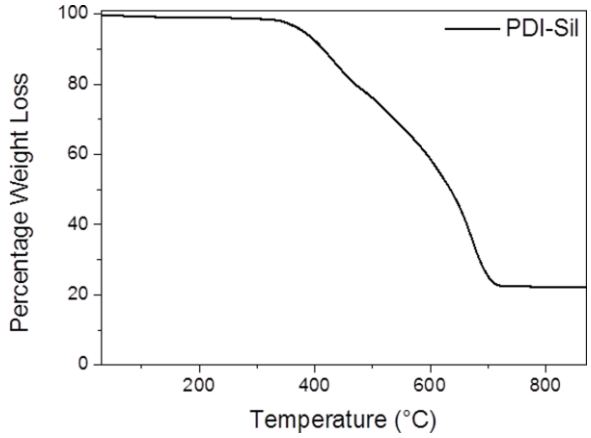

Figure S11. TGA of **PDI-Sil** (air atmosphere, 10° C min^{-1}).

The thermal degradation of **PDI-Sil** occurs in a two steps process: the first weight loss (onset T~380 °C) corresponds to the degradation of the alkyl chains bounded to the nitrogen atom, while the second weight loss is ascribed to the thermal decomposition of the aromatic backbone (onset T~621 °C).

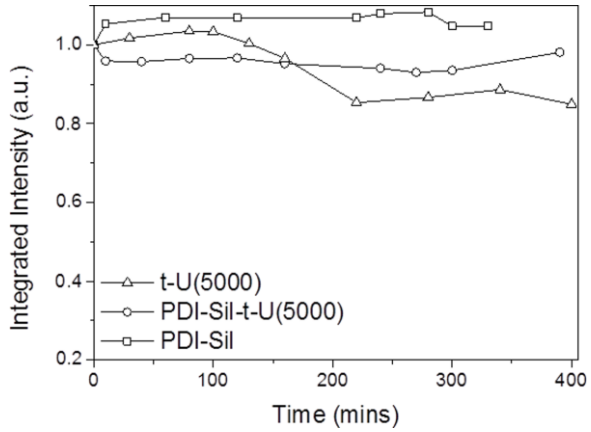

Figure S12. Integrated emission intensity of a **t-U(5000)** (open triangles), **PDI-Sil-t-U(5000)** (open circles) and a **PDI-Sil** thin film irradiated at 370 nm. The solid lines serve only to guide the eye.

Photostability studies were performed on a **t-U(5000)** monolith, a **PDI-Sil-tU(5000)** monolith and a thin film of pure **PDI-Sil** dye obtained by spin coating a solution the dye (10 mg cm^{-3} in THF) onto a cleaned glass slide at a rate of 2000 rpm. Samples were irradiated with a Xe arc lamp (450 W) for over 5 hours (λ_{exc} = 370 nm), using the same experimental configuration used while performing PL measurements. The irradiation of the source was measured using a photodiode (Newport, 818-VU-L detector) coupled to a Keithley 2401 Sourcemeter in two probe mode with Tracer2 software, yielding a value of 0.5476 W/m^2 at 370 nm.

6. Steady-State Photoluminescence (PL) Studies

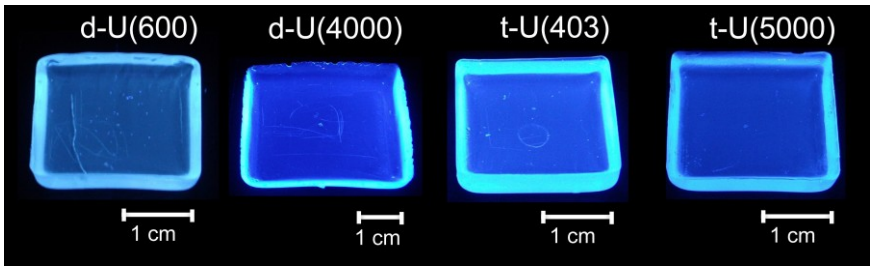

Figure S13. Photographs of undoped ureasils under UV excitation (λ_{ex} = 365 nm).

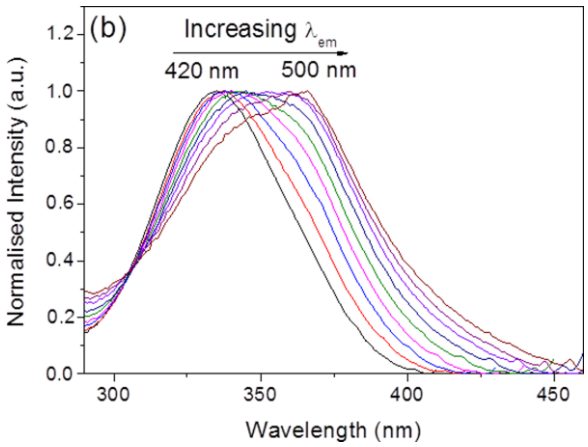

Figure S14. Excitation spectra of **t-U(403)** as a function of emission wavelength.

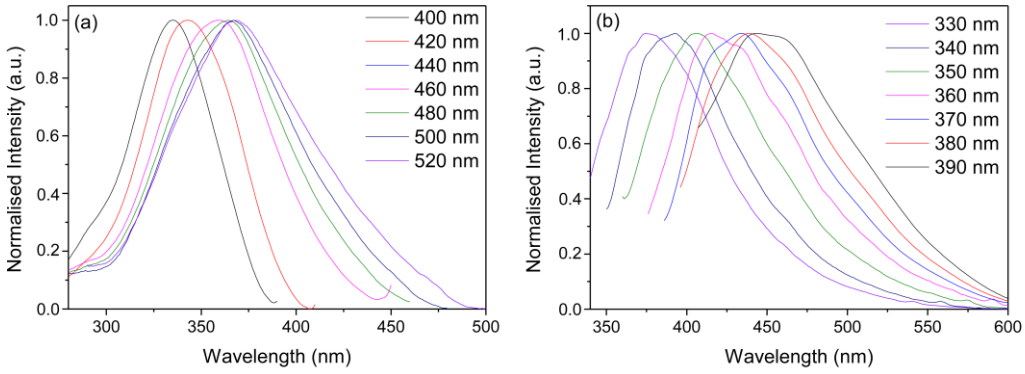

Figure S15. (a) Excitation and (b) photoluminescence spectra of **d-U(600)** as a function of emission and excitation wavelength, respectively.

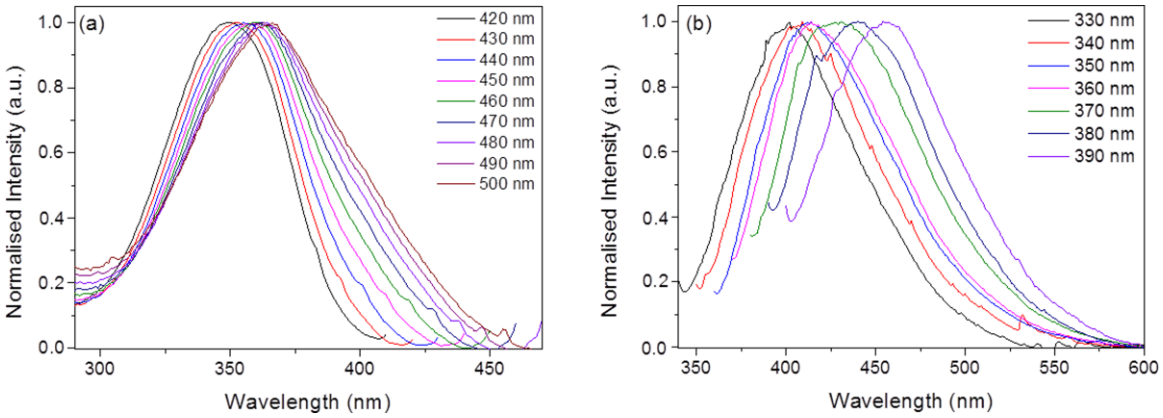

Figure S16. (a) Excitation and (b) photoluminescence spectra of **d-U(4000)** as a function of emission and excitation wavelength, respectively.

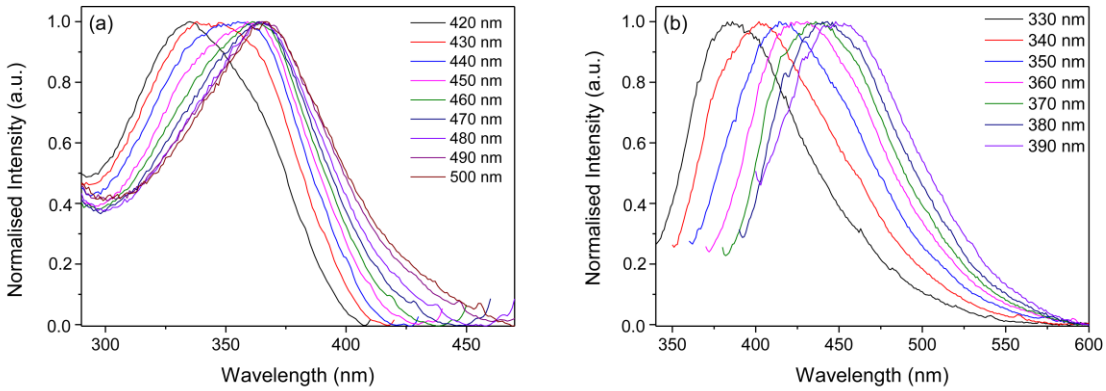

Figure S17. (a) Excitation and (b) photoluminescence spectra of **t-U(5000)** as a function of emission and excitation wavelength, respectively.

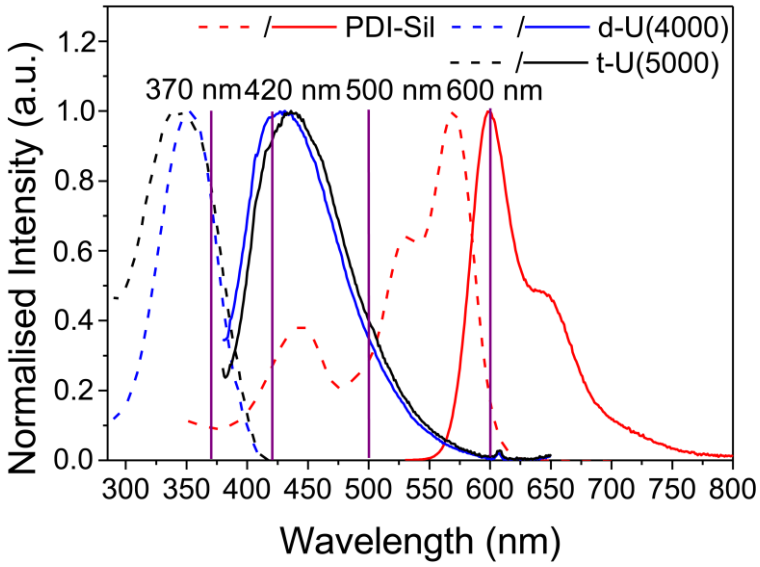

Figure S18. Emission and excitation spectra for **t-U(5000)** (black, λ_{ex} = 370 nm, λ_{em} = 420 nm), **d-U(4000)** (blue, λ_{ex} = 365 nm, λ_{em} = 420 nm) and UV/Vis absorption and emission spectra for **PDI-Sil** (red, λ_{ex} = 590 nm in THF). Emission spectra are shown as solid lines and excitation and UV-Vis absorption spectra are shown as dashed lines. The purple lines highlight the excitation (λ_{ex}) and emission (λ_{em}) wavelengths used in the TCSPC experiments.

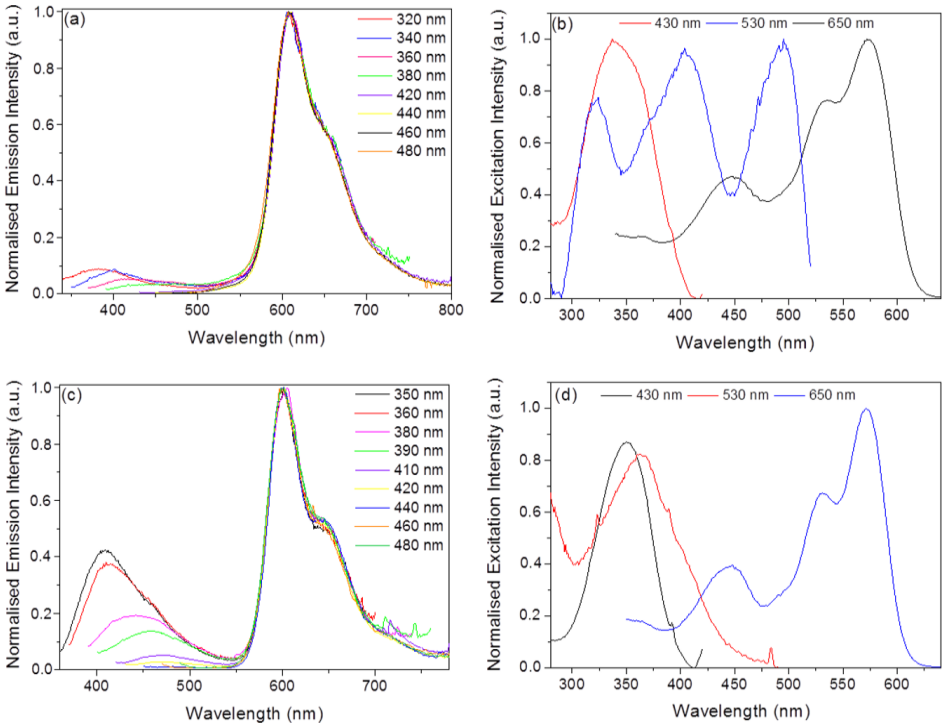

Figure S19. Emission spectra of (a) **PDI-Sil-d-U(600)** and (c) **PDI-Sil-d-U(4000)** and excitation spectra of (b) **PDI-Sil-d-U(600)** and (d) **PDI-Sil-d-U(4000)** spectra as a function of excitation and emission wavelength, respectively.

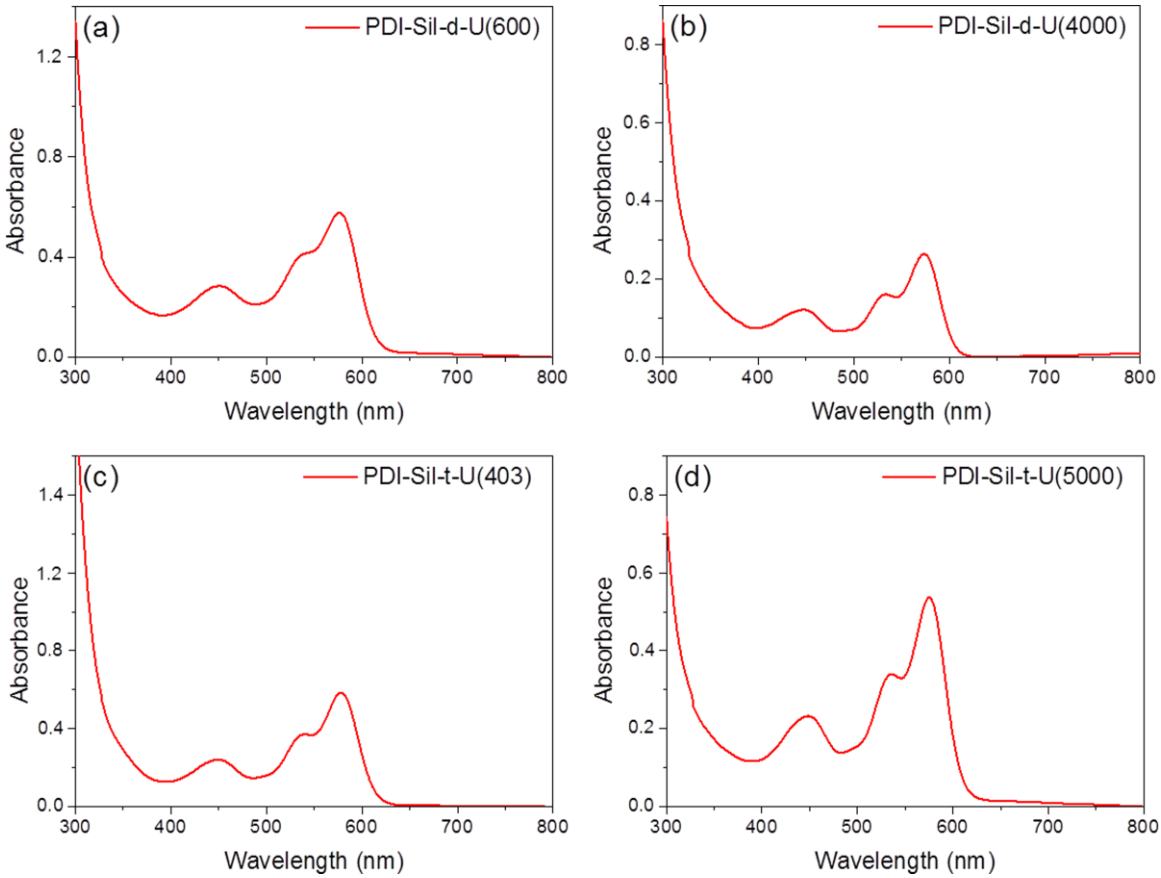

Figure S20. UV-Vis absorption spectra of monoliths of (a) **PDI-Sil-d-U(600)**, (b) **PDI-Sil-d-U(4000)**, (c) **PDI-Sil-t-U(403)** and (d) **PDI-Sil-t-U(5000)**.

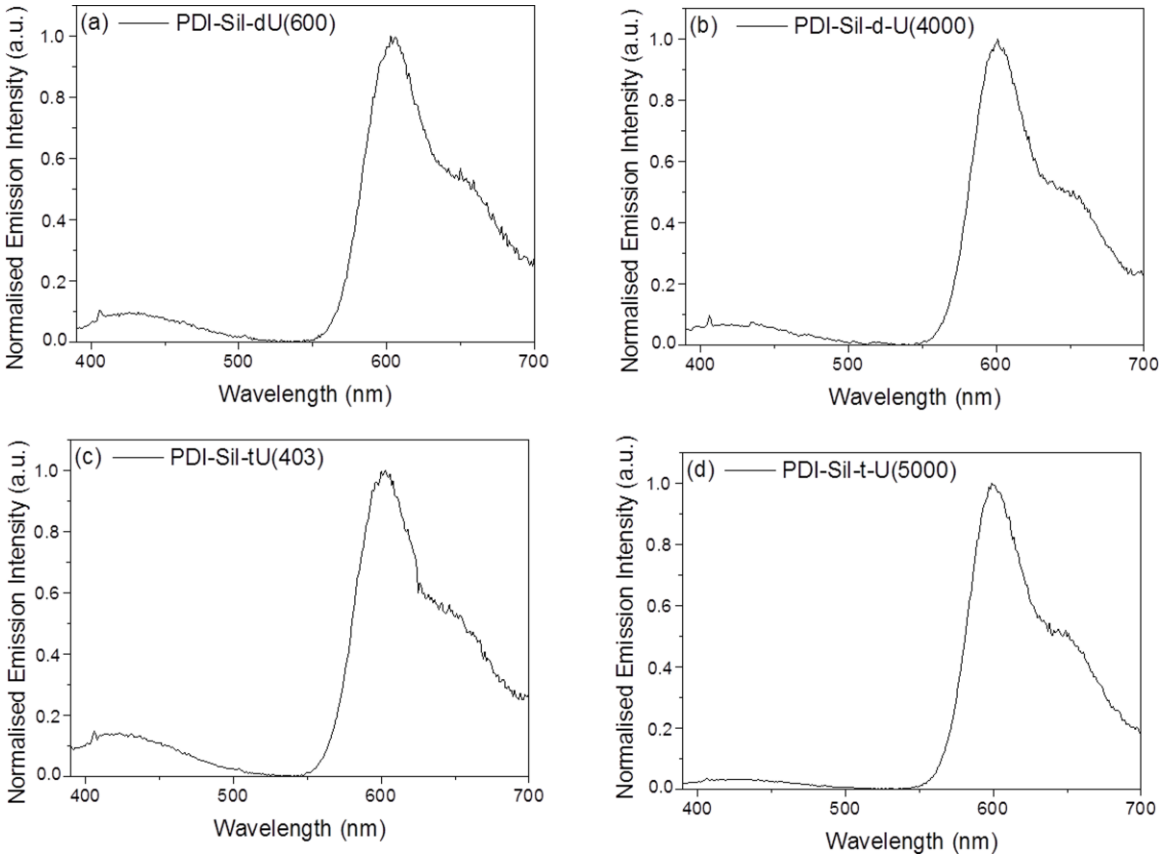

Figure S21. Emission spectra (λ_{ex} = 370 nm) of films of (a) **PDI-Sil-d-U(600)**, (b) **PDI-Sil-d-U(4000)**, (c) **PDI-Sil-t-U(403)** and (d) **PDI-Sil-t-U(5000)**.

Table S4. Measured photoluminescence quantum yields for **PDI-Sil**-ureasils (λ_{ex} = 520 nm).

Sample ID	Φ_{PL} (measured)[a]	Φ_{PL} (corrected)[b]
PDI-Sil-d-U(600)	76.3 (±1.1)	81.1
PDI-Sil-d-U(4000)	86.7 (±4.4)	88.2
PDI-Sil-t-U(403)	77.7 (±1.2)	83.8
PDI-Sil-t-U(5000)	83.4 (±0.3)	87.0

[a] Average of three independent measurements
[b] Corrected for reabsorption effects according to the method described in ref [2].

7. Picosecond time-resolved emission decays – data fitting procedure and results

Fluorescence decays were measured for undoped ureasils and PDI-Sil-ureasils, upon excitation at 370 nm to enable (semi-)selective excitation of the ureasil. The emission was detected as 420 nm and 500 nm to monitor the ureasil contribution and at 600 nm to isolate the **PDI-Sil** emission. In the ureasil detection range, the decay curves for all samples displayed complex multi-exponential behaviour, requiring a minimum of three exponential components to fit the data. The form of the theoretical multi-exponential decay is given by:

$$I(t) = \sum_i \alpha_i \exp\left(-t/\tau_i\right) \tag{1}$$

where α_i and τ_i are the pre-exponential factor and characteristic lifetime for component i, respectively. This is the theoretical expression for the response of a sample to an infinitely sharp excitation, also known as a δ-function.[3] In this model, the intensity is assumed to decay as the sum of individual single exponential decays. When examining a single fluorophore displaying a complex decay it is generally safe to assume that the fluorophore has the same radiative decay rate in each environment. Thus, in this case α_i represents the fraction of molecules in each environment at $t = 0$.[4]

The fractional contribution f_i of each decay component to the steady-state intensity can be calculated from:

$$f_i = \frac{\alpha_i \tau_i}{\sum \alpha_i \tau_i} \tag{2}$$

where $\alpha_i \tau_i$ is the area under the decay curve for each decay component.

The average fluorescence lifetime $<\tau>$ can be calculated from:

$$<\tau> = \frac{\sum \alpha_i \tau_i^2}{\sum \alpha_i \tau_i} \tag{3}$$

In reality the excitation pulse is not an infinitely short δ-function and thus the sample does not only decay starting directly after the pulse. Thus, the theoretical sample decay (1) must be reconvoluted with the instrumental response function (IRF) (which includes the width of the excitation pulse and possible electronic responses of the instrument) in the form:

$$I'(t) = \int_0^t E(t')I(t-t')dt' \tag{4}$$

where *E(t)* is the excitation pulse and *I(t)* is the theoretical decay model (1). This expression states that the experimentally measured intensity at time *t* is given by the sum of the intensities expected for all δ-function excitation pulses that occur until time *t,* if the excitation pulse is imagined to be comprised as a series of δ-functions with different amplitudes.[5] This model is then fit to the measured decay through the method of non-linear least squares analysis. This is achieved by varying α_i and τ_i until χ^2 is at a minimum. χ^2 is the goodness-of-fit parameter and is described by:

$$\chi^2 = \sum_{i=1}^{n} \left[\frac{y_i - f_{ic}}{y_i^2} \right]^2 \tag{5}$$

where y_i is the measured data, n is the number of data points and f_{ic} is the calculated fit. As α_i and τ_i are varied according to the χ^2 of the previous fit, this method is known as iterative reconvolution. The quality of the non-linear least squares analysis was also judged based on the randomness of the residuals plot. Residuals are the vertical deviation of the measured data points from the fitted curve. Non-random behaviour in the residuals plot suggests a poor fit or a hidden variable.

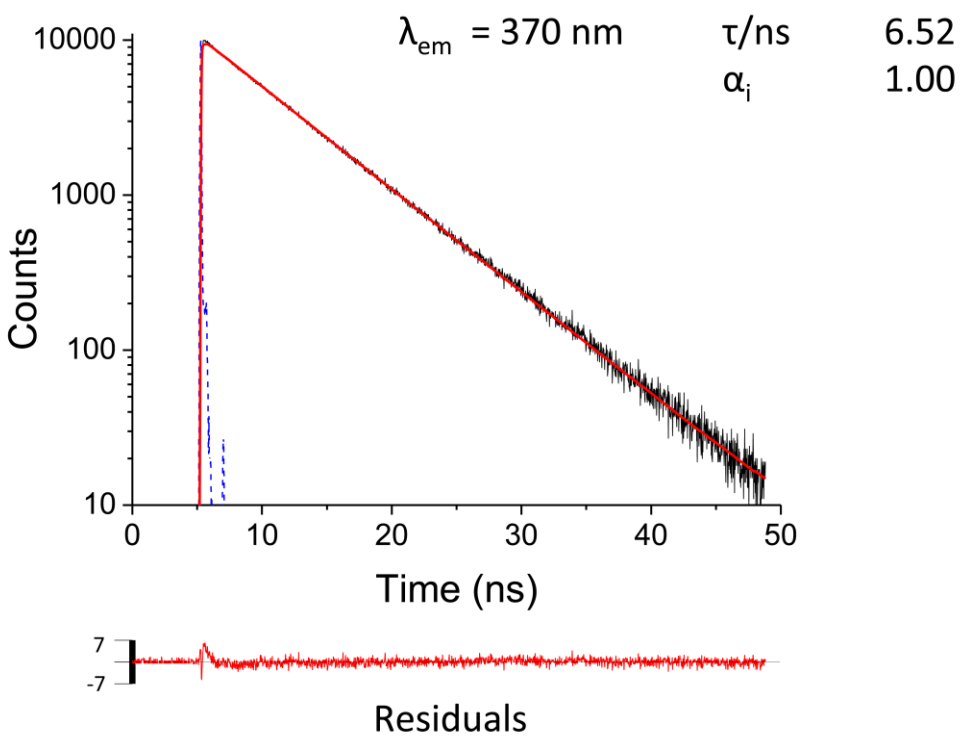

Figure S22. Photoluminescence decay for **PDI-Sil** in THF (Abs ~0.1 at 460 nm). The resulting decay time (τ), fit, weighted residuals (WR) and IRF are also shown.

Table S5. Photoluminescence (PL) lifetimes (τ_i), pre-exponential coefficients (α_i), fractional contribution (f_i) and chi squared (χ^2) values obtained from fitting of the emission decays (λ_{ex} = 370 nm) of undoped ureasils at λ_{em} = 420 and 500 nm.

Sample	τ_1 (ns)	τ_2 (ns)	τ_3 (ns)	α_1	α_2	α_3	f_1	f_2	f_3	χ^2
					λ_{em} = 420 nm					
t-U(403)	0.53 ± 0.03	4.28 ± 0.05	12.90 ± 0.09	0.49 ± 0.22	0.40 ± 0.09	0.11 ± 0.05	0.08 ± 0.03	0.50 ± 0.10	0.42 ± 0.17	1.42
t-U(5000)	0.49 ± 0.03	3.11 ± 0.04	9.22 ± 0.07	0.47 ±0.04	0.39 ± 0.03	0.15 ± 0.03	0.08 ± 0.01	0.43 ± 0.05	0.48 ± 0.11	1.39
d-U(4000)	0.71 ± 0.03	3.91 ± 0.05	9.84 ± 0.07	0.48 ± 0.04	0.36 ± 0.04	0.16 ±0.04	0.10 ± 0.01	0.43 ± 0.06	0.47 ±0.11	1.24
d-U(600)	0.47 ± 0.01	2.56 ± 0.04	10.08 0.12	0.75 ±0.02	0.20 ± 0.01	0.05 ± 0.01	0.24 ± 0.03	0.40 ± 0.05	0.36 ± 0.11	1.55
					λ_{em} = 500 nm					
t-U(403)	1.00 ± 0.05	5.53 ± 0.06	15.68 ± 0.15	0.46 ± 0.06	0.43 ± 0.06	0.11 ± 0.05	0.10 ± 0.02	0.52 ± 0.10	0.38 ± 0.17	1.28
t-U(5000)	0.71 ± 0.04	4.45 ± 0.05	11.17 ± 0.08	0.39 ± 0.05	0.43 ± 0.05	0.17 ± 0.04	0.07 ± 0.01	0.46 ± 0.07	0.47 ± 0.13	1.15
d-U(4000)	0.85 ± 0.06	5.39 ± 0.06	12.72 ±0.10	0.39 ± 0.06	0.43 ± 0.06	0.18 ± 0.05	0.07 ± 0.01	0.46 ± 0.09	0.47 ± 0.15	1.24
d-U(600)	0.39 ± 0.02	2.79 ± 0.05	10.90 ± 0.14	0.63 ± 0.03	0.29 ± 0.02	0.07 ± 0.02	0.13 ± 0.02	0.44 ± 0.06	0.43 ± 0.13	1.66

Table S6. PL lifetimes (τ_i), pre-exponential coefficients (α_i), fractional contribution (f_i) and chi squared (χ^2) values obtained from fitting of the emission decays (λ_{ex} = 370 nm) of PDI-Sil-ureasils at λ_{em} = 420 and 500 nm.

Sample	τ_1 (ns)	τ_2 (ns)	τ_3 (ns)	α_1	α_2	α_3	f_1	f_2	f_3	χ^2
					λ_{em} = 420 nm					
PDI-Sil-t-U(403)	0.56 ± 0.03	4.53 ± 0.06	13.79 ± 0.09	0.46 ± 0.05	0.39 ± 0.05	0.15 ± 0.04	0.06 ± 001	0.42 ± 0.08	0.51 ± 0.16	1.40
PDI-Sil-t-U(5000)	0.73 ± 0.02	3.19 ± 0.04	9.18 ± 0.07	0.58 ± 0.04	0.31 ± 0.03	0.11 ± 0.03	0.17 ± 0.02	0.40 ±0.05	0.43 ± 0.10	1.15
PDI-Sil-d-U(4000)	0.58 ± 0.03	3.79 ± 0.04	9.78 ± 0.07	0.46 ± 0.04	0.38 ± 0.04	0.16 ± 0.03	0.08 ± 0.01	0.44 ± 0.06	0.47 ± 0.11	1.17
PDI-Sil-d-(600)	0.42 ± 0.01	2.03 ± 0.04	8.06 ± 0.11	0.71 ± 0.03	0.24 ± 0.01	0.05 ± 0.01	0.24 ± 0.02	0.40 ± 0.04	0.36 ± 0.09	1.55
					λ_{em} = 500 nm					
PDI-Sil-t-U(403)	1.03 ± 0.04	5.02 ± 0.05	15.06 ± 0.10	0.48 ± 0.06	0.40 ± 0.05	0.12 ± 0.05	0.11 ± 0.02	0.46 ± 0.09	0.43 ± 0.17	1.17
PDI-Sil-t-U(5000)	0.86 ± 0.03	4.60 ± 0.05	11.66 ± 0.09	0.49 ± 0.05	0.38 ± 0.05	0.13 ± 0.04	0.11 ± 0.02	0.47 ± 0.08	0.41 ± 0.13	1.10
PDI-Sil-d-U(4000)	0.78 ± 0.05	4.98 ± 0.05	12.47 ± 0.07	0.36 ± 0.06	0.44 ± 0.06	0.21 ± 0.05	0.06 ± 0.01	0.43 ± 0.08	0.52 ± 0.14	1.13
PDI-Sil-d-(600)	0.62 ± 0.02	3.31 ± 0.04	10.28 ± 0.09	0.53 ± 0.04	0.38 ± 0.03	0.09 ± 0.03	0.13 ± 0.02	0.49 ± 0.06	0.38 ± 0.11	1.24

8. Steady-state fluorescence anisotropy measurements

The fluorescence anisotropy, <*r*>, is determined from:

$$< r >= \frac{\boldsymbol{I_{\parallel} - GI_{\perp}}}{\boldsymbol{I_{\parallel} + 2GI_{\perp}}} \quad (4)$$

where $I_{\parallel}$ and $I_{\perp}$ are the fluorescence intensities of the vertically (∥) and horizontally (⊥) polarised emission when the sample is excited with vertically polarised light. Only fluorophores with a component of their absorption transition dipole moments parallel to the incoming polarized light can undergo absorption. This phenomenon is known as photoselection, and it is only from this sub-set of the molecular population that fluorescence can subsequently occur. In a perfectly aligned, rigid system in which the absorption and emission transition dipole moments are colinear, photoselection will result in highly polarized emission and the anisotropy takes a maximum value of 0.4. Fluorescence depolarisation can result from a variety of factors including rotational diffusion, reabsorption and scattering.

The *G* factor corrects for the anisotropic nature of the emission polariser and is given by $G = I_{hv}/I_{hh}$, where $I_{\text{ex,em}}$ is the emission intensity and *v* and *h* denote the vertical and horizontal alignment of the polarisers. *G* is experimentally determined by recording the polarised emission from a totally isotropic solution whose emission spectrum coincides with the system under investigation. The *G* factor was measured for a dilute solution of **PDI-Sil** in THF and was found to be independent of excitation wavelength.

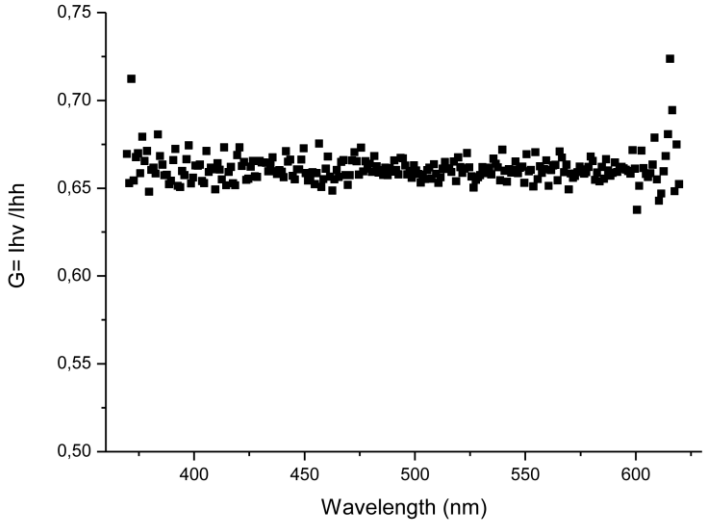

Figure S23. Calculated *G* values for a dilute solution of **PDI-Sil** in THF (λ_{em} = 630 nm).

9. References

[1] P. P. Lima, R. A. S. Ferreira, S. A. Júnior, O. L. Malta, L. D. Carlos, *J. Photochem. Photobiol. A*, 2009, **201**, 214.

[2] T.-S. Ahn, R. O. Al-Kaysi, A. M. Müller, K. M. Wentz and C. J. Bardeen, *Rev. Sci. Instrum.*, 2007, **78**, 086105.

[3] J. R. Lakowicz, in *Principles of Fluorescence Spectroscopy*, Springer, **2006**, p. 99.

[4] J. R. Lakowicz, in *Principles of Fluorescence Spectroscopy*, Springer, **2006**, p. 142.

[5] J. R. Lakowicz, in *Principles of Fluorescence Spectroscopy*, Springer, **2006**, p. 106.